Full text at publisher | Export | Add To Marked List

Modeling of temperature-dependent photoluminescence of GaN epilayer by artificial neural network

By: Tüzemen, ES (Tuzemen, Ebru Senadim) [1], [2] ; Yüksek, AG (Yuksek, Ahmet Gurkan) [3] ; Demir, I (Demir, Ilkay) [2], [4] ; Horoz, S (Horoz, Sabit) [2], [5] ; Altuntas, I (Altuntas, Ismail) [2], [4]

Source: JOURNAL OF THE AUSTRALIAN CERAMIC SOCIETY
DOI: 10.1007/s41779-023-00911-w

Early Access: JUN 2023

Indexed: 2023-07-04

Document Type: Article; Early Access

Jump to: ↓Enriched Cited References

Abstract: Artificial neural networks (ANNs) are a type of machine learning model that are designed to mimic the structure and function of biological neurons. They are particularly well-suited for tasks such as image and speech recognition, natural language processing, and prediction tasks. The success of an ANN in modeling a particular dataset depends on factors such as the size and quality of the dataset, the complexity of the model, and the choice of training algorithms. High representation rate of a system in the data set can improve the performance of the ANN model. The study we described is focused on using artificial neural networks (ANNs) to model temperature-dependent photoluminescence (PL) characterization of GaN epilayers grown on patterned sapphire substrates (PSS) using the metalorganic chemical vapor deposition (MOCVD) technique. The ANN model is trained using temperature and wavelength as input parameters and intensity as the output parameter, with the goal of accurately predicting the PL intensity of the GaN epilayer as a function of temperature and wavelength. The model is trained using a large set of experimental data and then tested using data that was not presented to the model during training. The results of the study suggest that ANN modeling methodology is an effective and accurate way of modeling temperature-dependent PL of GaN epilayers grown on PSS. The results of the study suggest that ANN modeling methodology can be used to accurately predict the temperature-dependent PL of GaN epilayers grown on PSS. This means that it may be possible to reduce the number of required experimental measurements by using the ANN model to predict PL intensity at different temperatures, based on a smaller set of experimental measurements. This could potentially save time and resources, while still obtaining accurate information about the optical behavior of GaN-based materials at different temperatures.

Citation Network

In Web of Science Core Colle

0 Citations

Create citation alert

51 Cited References

View Related Records →

Use in Web of Science

5 Last 180 Days

5 Sin

Learn more →

This record is from:

Web of Science Core Collec

- Science Citation Index Exp EXPANDED)

Suggest a correction

Journal information

JOURNAL OF THE AUSTRALIAN CERAMIC SOCIETY

Publisher name: SPRINGER

Journal Impact Factor ™

1.9 (2022)

1.7 (Five Year)

JCR Category	Category Rank	Category Quartile
MATERIALS SCIENCE, CERAMICS *in SCIE edition*	13/29	Q2

Source: Journal Citation Reports 2022. Learn more

Journal Citation Indicator ™

0.43 (2022)

0.41 (2021)

JCI Category	Category Rank	Category Quartile
MATERIALS SCIENCE, CERAMICS *in SCIE edition*	13/30	Q2

The Journal Citation Indicator is a measure of the average Category Normalized Citation Impact (CNCI) of citable items (articles and reviews) published by a journal over a recent three year period. It is used to help you evaluate journals based on other metrics besides the Journal Impact Factor (JIF).

Learn more

Interested in reviewing for this journal?

Add this journal to your reviewer interest list. Add Journal

Filters Clear All

- *Web of Science* Coverage
- Open Access
- Category
- Country / Region
- Language
- Frequency
- Journal Citation Reports

Refine Your Search Results

Journal of the Australian Ceramic Society Search

Sort By: Relevancy

Search Results

Found 929 results (Page 1) Share These Results

Exact Match Found

JOURNAL OF THE AUSTRALIAN CERAMIC SOCIETY

Publisher: **SPRINGER , ONE NEW YORK PLAZA, SUITE 4600 , NEW YORK, United States, NY, 10004**

ISSN / eISSN: **2510-1560 / 2510-1579**

Web of Science Core Collection: **Science Citation Index Expanded**

Additional *Web of Science* Indexes: **Current Contents Engineering, Computing & Technology | Essential Science Indicators**

Share This Journal View profile page

** Requires free login.*

Other Possible Matches

AMERICAN CERAMIC SOCIETY BULLETIN

Publisher: **AMER CERAMIC SOC , 600 N CLEVELAND AVE, WESTERVILLE, USA, OH, 43082**

ISSN / eISSN: **0002-7812 / 1945-2705**

Web of Science Core Collection: **Science Citation Index Expanded**

Additional *Web of Science* Indexes: **Current Contents Engineering, Computing & Technology | Current Contents Physical, Chemical & Earth Sciences | Essential Science Indicators**

Share This Journal View profile page

** Requires free login.*

JOURNAL OF THE CERAMIC SOCIETY OF JAPAN

Publisher: CERAMIC SOC JAPAN-NIPPON SERAMIKKUSU KYOKAI , 22-17, HYAKUNIN-CHO 2-CHOME, SHINJUKU-KU, TOKYO, JAPAN, 169-0073

ISSN / eISSN: 1882-0743 / 1348-6535

Web of Science Core Collection: Science Citation Index Expanded

Additional *Web of Science* Indexes: Current Contents Engineering, Computing & Technology | Current Contents Physical, Chemical & Earth Sciences | Essential Science Indicators

Share This Journal | View profile page

* Requires free login.

JOURNAL OF THE AMERICAN CERAMIC SOCIETY

Publisher: WILEY , 111 RIVER ST, HOBOKEN, USA, NJ, 07030-5774

ISSN / eISSN: 0002-7820 / 1551-2916

Web of Science Core Collection: Science Citation Index Expanded

Additional *Web of Science* Indexes: Current Contents Engineering, Computing & Technology | Current Contents Physical, Chemical & Earth Sciences | Essential Science Indicators

Share This Journal | View profile page

* Requires free login.

JOURNAL OF THE EUROPEAN CERAMIC SOCIETY

Publisher: ELSEVIER SCI LTD , 125 London Wall, London, England, EC2Y 5AS

ISSN / eISSN: 0955-2219 / 1873-619X

Web of Science Core Collection: Science Citation Index Expanded

Additional *Web of Science* Indexes: Current Contents Engineering, Computing & Technology | Current Contents Physical, Chemical & Earth Sciences | Essential Science Indicators

Share This Journal | View profile page

* Requires free login.

JOURNAL OF THE KOREAN CERAMIC SOCIETY

Publisher: SPRINGER HEIDELBERG , TIERGARTENSTRASSE 17, HEIDELBERG, GERMANY, D-69121

ISSN / eISSN: 1229-7801 / 2234-0491

Web of Science Core Collection: Science Citation Index Expanded

Additional *Web of Science* Indexes: Current Contents Engineering, Computing & Technology | Essential Science Indicators

Share This Journal | View profile page

* Requires free login.

TRANSACTIONS OF THE INDIAN CERAMIC SOCIETY

Publisher: **TAYLOR & FRANCIS LTD , 2-4 PARK SQUARE, MILTON PARK, ABINGDON, England, OXON, OX14 4RN**

ISSN / eISSN: **0371-750X / 2165-5456**

Web of Science Core Collection: **Science Citation Index Expanded**

Additional *Web of Science* Indexes: **Essential Science Indicators**

Share This Journal | View profile page

* Requires free login.

BULLETIN OF THE AUSTRALIAN MATHEMATICAL SOCIETY

Publisher: **CAMBRIDGE UNIV PRESS , EDINBURGH BLDG, SHAFTESBURY RD, CAMBRIDGE, ENGLAND, CB2 8RU**

ISSN / eISSN: **0004-9727 / 1755-1633**

Web of Science Core Collection: **Science Citation Index Expanded**

Additional *Web of Science* Indexes: **Essential Science Indicators**

Share This Journal | View profile page

* Requires free login.

JOURNAL OF THE AUSTRALIAN MATHEMATICAL SOCIETY

Publisher: **CAMBRIDGE UNIV PRESS , EDINBURGH BLDG, SHAFTESBURY RD, CAMBRIDGE, ENGLAND, CB2 8RU**

ISSN / eISSN: **1446-7887 / 1446-8107**

Web of Science Core Collection: **Science Citation Index Expanded**

Additional *Web of Science* Indexes: **Current Contents Physical, Chemical & Earth Sciences | Essential Science Indicators**

Share This Journal | View profile page

* Requires free login.

JOURNAL OF ASIAN CERAMIC SOCIETIES

OPEN ACCESS

Publisher: **TAYLOR & FRANCIS LTD , 2-4 PARK SQUARE, MILTON PARK, ABINGDON, England, OXON, OX14 4RN**

ISSN / eISSN: **2187-0764**

Web of Science Core Collection: **Science Citation Index Expanded**

Additional *Web of Science* Indexes: **Current Contents Engineering, Computing & Technology | Current Contents Physical, Chemical & Earth Sciences | Essential Science Indicators**

Share This Journal | View profile page

* Requires free login.

Journal of the Australian Ceramic Society (2023) 59:1145–1159
https://doi.org/10.1007/s41779-023-00911-w

RESEARCH

Modeling of temperature-dependent photoluminescence of GaN epilayer by artificial neural network

Ebru Şenadım Tüzemen[1,2] · Ahmet Gürkan Yüksek[3] · İlkay Demir[2,4] · Sabit Horoz[2,5] · İsmail Altuntaş[2,4]

Received: 23 January 2023 / Revised: 5 June 2023 / Accepted: 11 June 2023 / Published online: 22 June 2023

Abstract

Artificial neural networks (ANNs) are a type of machine learning model that are designed to mimic the structure and function of biological neurons. They are particularly well-suited for tasks such as image and speech recognition, natural language processing, and prediction tasks. The success of an ANN in modeling a particular dataset depends on factors such as the size and quality of the dataset, the complexity of the model, and the choice of training algorithms. High representation rate of a system in the data set can improve the performance of the ANN model. The study we described is focused on using artificial neural networks (ANNs) to model temperature-dependent photoluminescence (PL) characterization of GaN epilayers grown on patterned sapphire substrates (PSS) using the metalorganic chemical vapor deposition (MOCVD) technique. The ANN model is trained using temperature and wavelength as input parameters and intensity as the output parameter, with the goal of accurately predicting the PL intensity of the GaN epilayer as a function of temperature and wavelength. The model is trained using a large set of experimental data and then tested using data that was not presented to the model during training. The results of the study suggest that ANN modeling methodology is an effective and accurate way of modeling temperature-dependent PL of GaN epilayers grown on PSS. The results of the study suggest that ANN modeling methodology can be used to accurately predict the temperature-dependent PL of GaN epilayers grown on PSS. This means that it may be possible to reduce the number of required experimental measurements by using the ANN model to predict PL intensity at different temperatures, based on a smaller set of experimental measurements. This could potentially save time and resources, while still obtaining accurate information about the optical behavior of GaN-based materials at different temperatures.

Keywords Artificial neural network · MOCVD · Photoluminescence · Semiconductor · Modeling

Introduction

III-Nitride compound semiconductors such as GaN, InN, AlN, and related alloys have gotten a lot of attention recently, and they have made remarkable development [1–3]. The fundamental explanation for this is that GaN and its alloys with AlN and InN have a wide range of applications in both electronic and optoelectronic devices [4]. GaN is a commonly utilized material for short-wavelength light-emitting diodes (LEDs), laser diodes (LDs), and photodetectors (PDs) that can be used in full-color displays and as a pumping source for white lightning LEDs [5–7]. High brightness GaN-based devices in the UV and green wavelengths are commercially available, but optical applications require more development [8]. GaN-based thin films are typically produced on a flat sapphire substrate [9]. The interface, however, leads to significant threading dislocation (TD) densities, which limit light output in optical devices because to the huge lattice

✉ Sabit Horoz
sabit.horoz@sivas.edu.tr

1 Department of Physics, Sivas Cumhuriyet University, 58140 Sivas, Turkey

2 Nanophotonics Research and Application Center, Sivas Cumhuriyet University, 58140 Sivas, Turkey

3 Computer Engineering Department, Sivas Cumhuriyet University, 58140 Sivas, Turkey

4 Department of Nanotechnology Engineering, Sivas Cumhuriyet University, 58140 Sivas, Turkey

5 Department of Metallurgical and Materials Engineering, Faculty of Engineering and Natural Sciences, Sivas University of Science and Technology, 58140 Sivas, Turkey

mismatch and thermal expansion coefficient discrepancies between the GaN and sapphire. Techniques for reducing dislocation density are critical for obtaining high-performance GaN-based devices [10, 11].

Several approaches [12–15] exist for reducing TD density and improving the crystalline quality of GaN epilayers produced on sapphire substrates. One of them is the epitaxial lateral overgrowth (ELOG) [16] which has been developed to reduce the TD density. The TD density was reduced less than 10^8 cm.$^{-2}$ using this overgrowth technique. To make an ELOG like this, first grow a 2–3-µm thick GaN epitaxial layer on a sapphire substrate, then shape the GaN epilayer, and create a second metalorganic chemical vapor deposition (MOCVD) [17, 18] layer on top of it. There is a considerable risk of impurity contamination and strain-induced defects in succeeding layer growth with this ELOG approach. This method includes a two-step MOCVD growth process. To overcome these issues, try using patterned sapphire substrate (PSS) with no lithographic steps and no suspension throughout growth process. High-quality GaN epilayers produced on PSS and similar nitride-based thin films with high output power have been reported [19–22]

GaN has a wurtzite structure in its native state and a large direct band gap of 3.4 eV at 300 K, allowing for efficient radiative recombination. By alloying or constructing heterostructures such as quantum wells with other nitrides, the wavelength of radiation from GaN-based materials can be adjusted over a wide range from visible to ultraviolet. Preparation and characterization of high-quality GaN produced using various growth procedures and development of GaN-based devices have all received a lot of attention [23].

The temperature dependency of optical properties of the GaN has been the subject of various studies [24–26]. The one of the efficient method to characterize optical properties of GaN epilayers is temperature dependent photoluminescence (PL) spectroscopy. However, the most important disadvantage of temperature-dependent PL measurements is that the laser source used in PL measurements is expensive and its lifetimes decrease over time. Therefore, it can be limiting to measure temperature-dependent PL in wide temperature ranges. The most effective way to eliminate this negative situation is to use machine learning technique. With this technique, it is possible to predict the behavior of temperature-dependent PL peaks without any experimental measurement necessity. Many studies have been reported on different applications of GaN-based thin films using machine learning technique. Torun et al. [27] conducted a study on the modeling of GaN-based Schottky diode characteristic with machine learning techniques based on experimental data in a wide temperature range. The work on optimizing GaN LEDs and reducing efficiency degradation using active machine learning was carried out by Humphreys et al. [17]. They concluded that this active learning strategy rapidly built a model of the devices that predicted Poisson-Schrödinger simulations and simultaneously produced structures with higher simulation efficiency. Wang et al. [28] proposed a machine learning supported model for GaN ohmic contacts for manufacturing processes. They stated that in the light of mature and powerful machine learning techniques, their work offered a new method to evaluate the fabrication processes of ohmic contacts in AlGaN/GaN heterojunction. Although there are different studies on GaN-based applications [29] with machine learning technique, no study has been found on the temperature-dependent PL characteristic of GaN thin films in the presence of machine learning technique until today. In terms of measurement and model, there is no limitation to apply to other semiconductors. Whenever the measurement result is obtained of the semiconductor sample, the proposed model can be applied to make some predictions even for semiconductors with high localized state density [30, 31]. In a previous study [32], an artificial neural network was used to model how the reflectance angle affects specular reflectance measurements of ZnO thin film. The model utilized a "Multi-Layer Perceptron (MLP)" and the back propagation algorithm, specifically Levenberg Marqued's learning rule within an incident angle range of 30–60 degrees. The study demonstrated that accurate and precise measurements can be obtained without the need for expensive hardware.

In this study, temperature-dependent PL characteristics of GaN epilayer grown on PSS by MOCVD were modeled by ANN for the first time. It was observed that there was an excellent agreement ($R^2 = 0.98$ for model-1, $R^2 = 0.98$ for model-2) between ANN model and experimental results.

Experimental details

Growth and characterization of GaN epilayer

The methodology of this study (shown in Fig. 1) consists of two work packages. These work packages include "epitaxial growth by MOCVD" and "characterization by PL."

GaN epilayer was grown by MOCVD on patterned sapphire substrate (PSS) which shaped as dome. NH_3, TMGa, and H_2 were used for N source, Ga source, and carrier gas, respectively. The sapphire substrate was desorbed just before the growth at the high temperature (~ 1080 °C) for 10 min in hydrogen environment to remove any surface contaminants. Epilayer growth of GaN started with nucleation layer on sapphire substrate just after desorption at 480 °C and 200 mbar. The reactor temperature was increased to above 1000 °C at the same reactor pressure to grow main GaN epilayer. Two -step GaN growth technique with different NH_3 flow rates was applied to have lower dislocation density epilayer [33, 34].

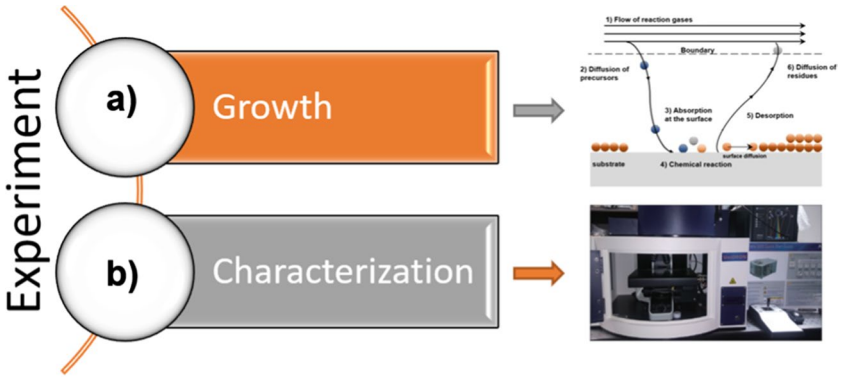

Fig. 1 The methodology of this study: (**a**) the processes steps at epitaxial growth and (**b**) the PL measurement system we used

Detailed temperature-dependent PL measurements were carried out for optical characterization of the GaN sample. PL measurements were carried out by the 325 nm HeCd laser which focused on the 10 × objective lens for fixed laser power. The power of the laser with 100 mW was adjusted as 10% by using ND (neutral-density) filters. The signal during the photoluminescence measurement was detected by the CCD detector and used 300 gr/mm 500 nm blaze grating.

Artificial neural networks (ANN)

An ANN is basically computational network, and the main objective is attempt to simulate the pattern recognition process in networks of neurons as same as the biological central nervous system with in special algorithms. This process is neuron to neuron simulation and working principle is based on the neurophysiological structure of biological neurons and network architecture of this biological neurons. So, the main computing principles of ANN differ from traditional computing (analog or digital) machines and aim to serve to change and increase or speed-up to the organization of the computing elements based on modeling of the human brain [35]. Another specialty of ANNs is the ability of parallel computations (a traditional computer is a sequential structured machine). A simple architecture of the neural element of ANN (neuron) is shown in Fig. 2, which is the well-known simple part of every ANN. It investigates the differences in the weighting of input signals at the diverse interconnections (synapses).

In the literature, many types of different neural networks have been studied, and it is observed that all of them have the basic and similar principles [36]. Every neuron in the network has the capability to get input signals, to process, and to forward as an output signals. Neuron in the network is connected minimum with one neighbor neuron, and every connection is represented by a real number, called the weight coefficient, that reflects the degree of significance of the given connection in the NN [38]. The basic idea is modeling the strong predictive or pattern recognition capability, in other words, representing a random mapping of one vector space into another vector space [39]. Thus, the most important advantage of neural networks is that they can detect some hidden patterns in the data. The process of obtaining the pattern recognition is described as "ANN learning" or "ANN training." Learning in mathematical form is accepted adjusting the weighting coefficients to model the system. Education is grouped under two main categories as supervised and unsupervised training. In supervised training, the neural networks have knowledge about the desired output, and the weighting factors are adjusted so that the desired and calculated output values are as close as possible. In unsupervised training, the desired output is

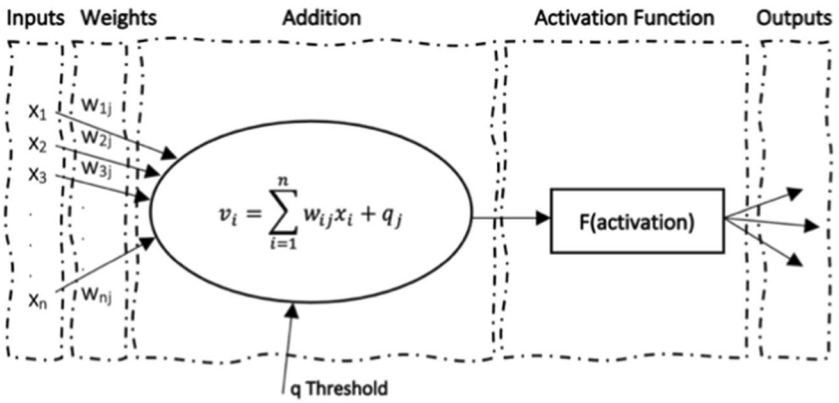

Fig. 2 A simple architecture of neuron [36]

unknown by the networks, and a set of facts (patterns) are presented to the system and then left alone to settle (or not) into a steady-state in some cases number of iterations [38]. The most widely used learning algorithm in many different applications of ANN is the "Backpropagation Algorithm (BPA)." It is the most preferred learning algorithm because it is easy to understand and can be proved mathematically. This algorithm is called backpropagation since it tries to reduce the errors backwards from the output to the input. There are three basic operations that occur on the networks trained using the back propagation learning algorithm: the training input data set is fed in forward direction to the network, the total error is calculated between the desired and calculated outputs and back propagated on the network, and the weights are rearranged [40]. The standard multiple backpropagation network always has an input, an output, and at least one hidden layer (Fig. 3). There is no accepted theoretical limitation about the number of hidden layers in network. Backpropagation algorithm is a general algorithm that falls under the supervised class of neural network. Any neuron in a specified layer is linked to all neurons in the next layer. The link between the I^{th} and j^{th} neurons is defined by the weight coefficient w_{ij} and the I^{th} neuron by the threshold coefficient v_i (Fig. 3). The weight coefficients of weight reflects the degree of importance of the given connection in the neural network. The output value (activity) of the I^{th} neuron x_i is determined by the equation of "Addition" layer given in Fig. 2.

The primary objective behind the most supervised learning algorithms is updating the ANN weight coefficients and the bias term coefficients until the mean squared error (Eq. 1 and Eq. 2) between the output values predicted by the network and the desired output are less than tolerance (Fig. 4).

Backpropagation, which is also known as the generalized delta rule and is formed from the generalization of the

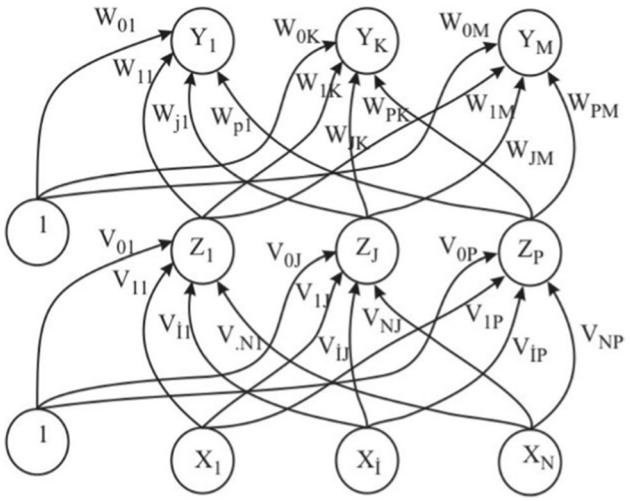

Fig. 3 Feedforward multilayer neural network architecture [36]

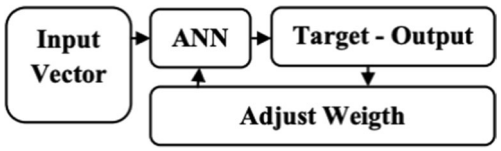

Fig. 4 ANN data analysis steps

Widrow-Hoff (least squares method) learning rule for multilayer networks, basically consists of two steps in its nature. In the first step, the input data is spread to the network (Y_{ij}) to calculate the network output value for each output unit through the input layers, hidden layers, output layers, and the existing connections between all these layers [41]. By comparing these calculated output values with the actual output values, the error value for each output cell is found. In the second step, these error values are presented to the network in the opposite direction and the updated necessary weights are calculated. The aim of the error back propagation method is to ensure that the total error of the network reaches its minimum value. Standard backpropagation is a gradient descent algorithm with the weights on the net moving at the negative part of the performance function slope. If the basic network operation equation is written for the unit (neuron) in the first hidden layer, represented by Z_1 in Fig. 3.

$$\begin{aligned} Z_{1-\text{Input}} &= x_1 v_{11} + .. + x_i v_{i1} + .. + x_N v_{N1} + v_{01} \\ Z_{J-\text{Input}} &= v_{0j} + \sum_{i=1}^{N} x_i v_{ij} \\ Z_{J-\text{Output}} &= f(Z|j - \text{Input}) \end{aligned} \tag{1}$$

As can be seen in Eq. 1, the output value, the neurons on a layer will produce, is the effect of the activation function of this neuron on the weighted sums of the neurons in the previous layer connected to it. The same equations are applied to the next layers. The created general model is given by Eq. 2.

$$a_{0:j}^{m} = \left(x_m\right)_j = x_j^m \tag{2a}$$

$$c_{i:j}^{m} = \sum_{k=1}^{s_{i-1}} w_{i:j,k} a_{i-1:k.}^{m} + b_{i:j} \ldots\ldots\ldots i > 0, \tag{2b}$$

$$a_{i:j}^{m} = F_{i:j}\left(c_{i:j}^{m}\right), \ldots\ldots\ldots\ldots\ldots i > 0 \tag{2I}$$

$$a_{i:j}^{m} = F_{i:j}\left(\sum_{k=1}^{s_{i-1}} w_{i:j,k} a_{i-1:k.}^{m} + b_{i:j}\right) \tag{2d}$$

$$a_{L:1}^{m} = y_m \tag{2I}$$

$$\frac{1}{2}\|y_m - t_m\|^2 = \frac{1}{2}\left(y_m - t_m\right)^2 = e_m^2 = \varepsilon_m \tag{2f}$$

Equality groups will be obtained. For I□1 in these equation groups, $\underline{a}_{i-1}^{m}$ response values are calculated for the layer I-1. It is presented to the network in the forward direction to determine the $\underline{a}_{i}^{m}$ response (computed) values required for the layer. Almost all of the training algorithms aim to ensure that the network output value is suitable with the intended values or the network error is small in line with the training sets presented to the network, and it is widely used with method parameters known as slope descent [42]. There are two most used approaches for slope calculation; the first approach is based on what is known as the chain rule, and the second approach is the backpropagation approach. The chain rule for multivariate structures is as expressed in Eq. 3.

$$\frac{df}{dt} = \frac{df}{dx}\frac{dx}{dt} \tag{3a}$$

$$\frac{df(g(x))}{dx} = \frac{df(z)}{dz}\lceil z \tag{3b}$$

In BPA, the steepest-descent minimization method is used. For adjustment of the threshold coefficients and weights, it holds as in Eq. 4.

$$\begin{aligned} w_{ij}^{(k+1)} &= w_{ij}^{(k)} - \lambda\left(\frac{\partial E}{\partial w_{ij}}\right)^{k} \\ v_{ij}^{(k+1)} &= v_{ij}^{(k)} - \lambda\left(\frac{\partial E}{\partial v_{ij}}\right)^{k} \end{aligned} \tag{4}$$

where □ is learning rate (0 > □ > 1). The main interest of problem is calculation of the derivatives $\frac{\partial E}{\partial w_{ij}}$ and $\frac{\partial E}{\partial v_{ij}}$ [35]. AANs have been described as powerful function approximators.

Superior features of ANN are due to having many model parameters of which values can be learned from data as mentioned via gradient descent focused optimization algorithm. In cases where the data set to be used for training is large, ANN is very successful in modeling the input–output relations, and with this aspect, it is a very effective method on the performance of tasks that will be considered as intelligent. In constraint, the flexibility of ANN has a deficit: they are especially sensitive to overfitting. Overfitting is the algorithm's ability to work through the training data to the lowest breakdown, memorize the results, and achieve success only on that data. The trained model starts to learn from observation that hidden patterns in the dataset. However, when models created in this way encounter new and previously unseen observations, they reduce your probability of making a successful prediction. The overfitting state is not unsolved problem for neural networks. Flexibility, one of the strengths of artificial intelligence, takes them particularly sensitive, and researchers have come up with many extensions to the known learning algorithm (early stopping, weight corruption, dropout, and so on) to reduce over-fitting [43]. Bayesian regularized artificial neural networks (BRANNs) are more powerful than known backpropagation algorithms net, and BRANN is a mathematical calculation that converts a non-linear regression into a fine-modeled statistical problem in the way of "a ridge regression." The most powerful side of BRANNs is that the models are strong and the validation steps, which balance in normal regression process, such as standard back propagation, are not necessary. BRANN supplies methods to a number of troubles such as choice, stability, choice of validation data set, size of validation effort, and standardization of NN architecture. The based advantage is difficult to overtrain BRANN method, since proof procedures supply a practical Bayesian criterion in stopping training. Furthermore, overfitting of this is hard because the BRANN calculates and trains on a number of influential network parameters or weights, effectively turning off those that are not suitable [44].

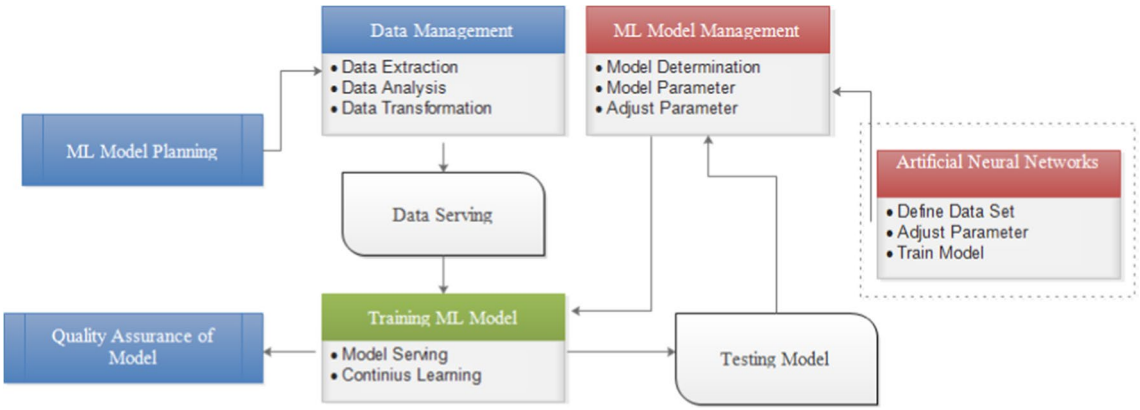

Fig. 5 ANN data analysis steps

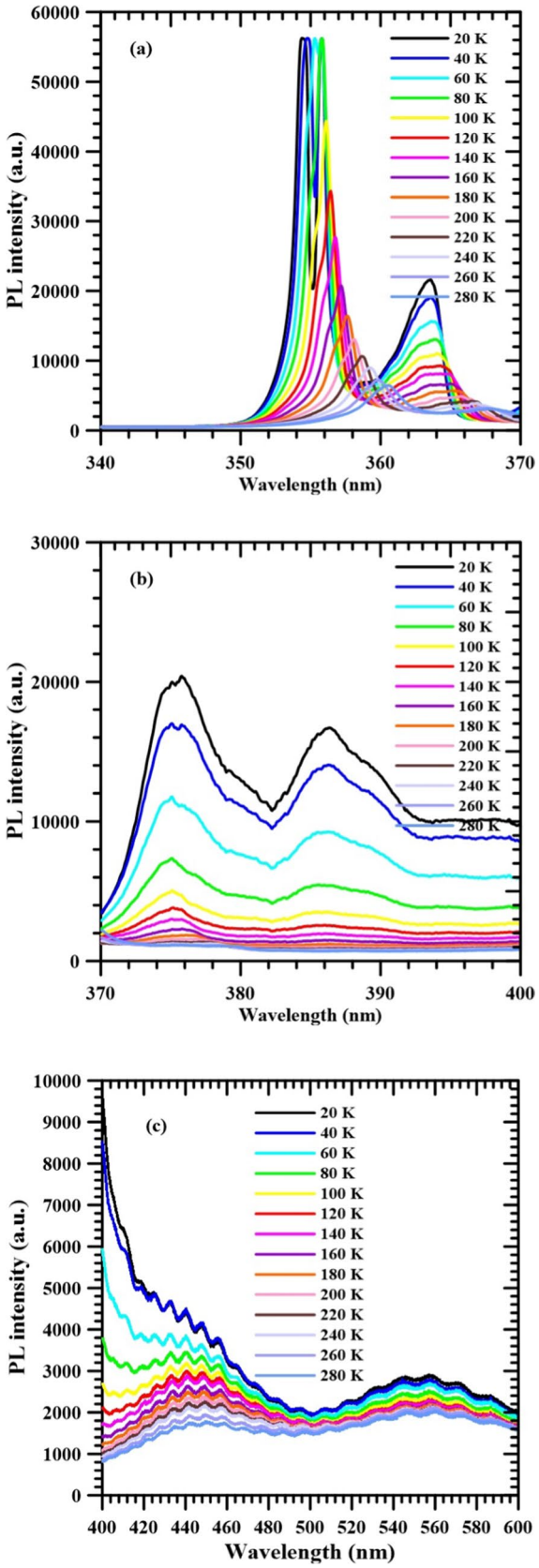

Fig. 6 The PL spectra (**a**) 340–370 nm, (**b**) 370–400 nm, and (**c**) 400–600 nm of GaN on PSS

Bayesian regularization-backpropagation neural network (BR-BPNN)

The classical backpropagation algorithmic aims to minimize the cost function $\sum_{i=1}^{n}(yi - ti)^2$, in this equation, "$n$" is the number of inputs in the training set, "y_i" is the "I_{th}" expected output, and "t_i" is the "I_{th}" output obtained as neural network response (Eq. 2-f). In general, if the scale of NN is much less than that of training data set, the possibility of overtraining is little. But, it is hard to determine the scale of NN. In order to get a NN with the most appropriate performance and minimal parameters and tide effectively, the problem of overfitting BRBPNN presents network weights into training objective function.

Regard a NN topology with training dataset named D having nt input and output vectors pairs in the NN model, in Eq. 5.

$$D = \left\{\left(u_1, t_{01}\right), \left(u_2, t_{02}\right), \ldots, \left(u_{nt}, t_{0nt}\right)\right\} \tag{5}$$

For every input (u) to the NN, the differentiation between goal output and estimated output is calculated as an error value I. In order to interpret the efficiency of the NN, i.e., how fine the NN performance is matching the testing set, a quantitative measurement is necessary. This measurement operation is called performance index of the NN and is used to optimize the NN design parameters. The standard performance index "F" is managed by the sum of the squared errors (SSE) in Eq. 6, where w indicates the vector of size k containing all the weights and biases of the network.

$$F\left(\overline{w}\right) = E_D = \sum_{i=1}^{n}\left(e_i\right)^2 = \sum_{i=1}^{nt}\left(y_{0i} - t_{0i}\right)^T\left(y_{0i} - t_{0i}\right) \tag{6}$$

To generalizing the NN, the performance index of Eq. 6 is changed using a regularization method. A penalty parameter "$(\mu\nu)E_W$" is added in the performance index $F(w)$, Eq. 7, where μ and v are the regularization parameters and E_w represents the sum of the squared network weights (SSW).

$$F\left(\overline{w}\right) = \mu\overline{w}^T\overline{w} + vE_D = \mu E_w + vE_D \tag{7}$$

Table 1 Dependent variable (input parameters)

Independent variable (input parameters)	
$X1$	Wavelength, nm
$X2$	Temperature, K
Dependent variable (output parameters)	
Y	Intensity, a.u

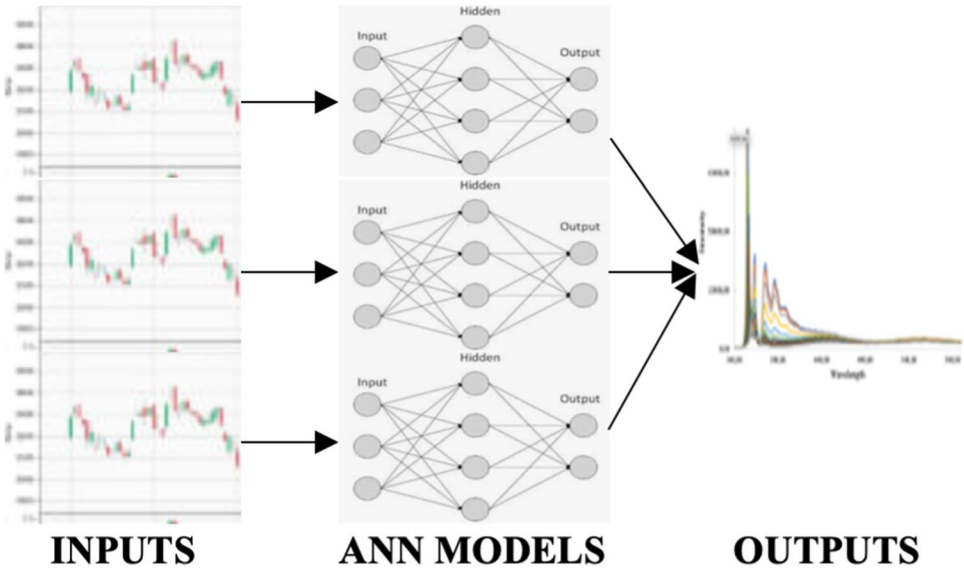

Fig. 7 Block diagram of developed model

Determining the optimum valuations for v and μ parameters is a challenging mission, as these parameter comparative values establish the basis for the training error. If $\mu << v$, less errors are generated, while if $\mu >> v$, there should be reduced weight size at the cost of network errors. For the aim of determining the optimum regularization values, a Bayesian regularization method is used [45]. When the trainings with BPNNRR ended, a less checks concerning the number of efficient parameters are necessary for preferable performance of the NN. The computing problem the Hessian matrix at the minimal point $\overline{w}$ is indirectly solved by Levenberg–Marquardt training algorithm (LM) while describing the minimum value of $F(\overline{w})$. By LM algorithm, the network weight values and bias values at the k^{th} iteration are described according to Eq. 8.

$$\overline{w}^{k+1} = \overline{w}^{k} - \left[J^{T}J + \lambda I\right]^{-1} J^{T}e \tag{8}$$

where λ denotes the Levenberg's damping factor, and $J^{T}e$ is the error gradient, which needs to be close to zero at end of the training [46].

A model establishment and preparation of the data set

The preparation of the database to be used for training is certainly the most influential factor in the success of the model during the design of the model's architecture in applications developed using artificial neural networks [47]. Complex data analysis operations performed with ANN models can be summarized as shown in Fig. 5.

From the perspective of systems analysis, the initial part of this flow is the stage in which the problem is defined, its limits are set, roadmaps are drawn, the flow is administratively created, and it is dominant over the processes of the whole model. The data set preparation in the second part is the creation of a data set that can respond to the results to be produced with the established model or system and model (represent) the problem in the best way. The structure and nature of the data set is very important for the model; it is the enlightening for decision makers about the problem as it will act as the trainer of the system to be trained. In the third stage, the ANN model, whose structure has been decided, is

Table 2 Model I train parameters

Hidden layer model	[5 10 20]
Train algorithm	Bayesian neural network
Momentum value	0.9
Train rate value	0.1
Train set temperature range (K)	[20 40 80 120 160 200 240 280]
Test set temperature range (K)	[60 100 140 180 220 260]
Data set wavelength range (nm)	[340–370]

Table 3 Model II train parameters

Hidden layer model	[5 10 20]
Train algorithm	Bayesian Neural Network
Momentum value	0.9
Train rate value	0.1
Train set temperature range (K)	[20 40 80 120 160 200 240 280]
Test set temperature range (K)	[60 100 140 180 220 260]
Data set wavelength range (nm)	[370 400]

trained by iterative operations. By performing data mining with the results produced by the ANN model, comparisons are made on with the real results and then the success of the model is tested [48].

Results and discussion

Experimental model definitions and obtained data from this model

Figure 6 demonstrates the temperature dependency of PL spectrum of GaN epilayer grown on PSS.

The emission that appeared around 362 nm at 280 K corresponds to free excitons and shallow donor bound excitons. The blue band emissions attribute to donor valance band transitions [20]. The yellow luminescence might be sourced for several reasons. It is known that the YL is most often attributed to defects such as either gallium vacancy (V_{Ga})-related defects or carbon (C)-related defects. Although initial calculations showed that V_{Ga} defects or $V_{GA}O_N$ complexes play an important role in the formation of YL, subsequent calculations predict that YL may be caused by isolated C defect, C_N, or C_NO_N complexes. Also, it is found that the YL can be sourced from $V_{Ga}O_N$-2H and V_{Ga}-3H complex [49]. The PL peak position of emission occurred at 280 K are 362 nm, 368 nm, 380 nm, 387 nm, and 550 nm. PL spectra of the GaN epilayer on PSS are dominated by band edge emission at 362 nm. The prominence of other peaks became much clearer with decreasing temperature resulting in increasing intensities of them. It is observed that there is a blue shift in the peak position of emissions at 362 nm, 368 nm, and 380 nm with decreasing temperature. A defect-related yellow luminescence peak which observed at around 550 nm is seen also the PL spectra of GaN on PSS. It is also observed that the increase in the intensity of this peak with decreasing temperature is much less than that of the other peaks [20]. The Fabry–Perot interference patterns have been observed in Fig. 6(b) due to the refractive index variations of the interface layers between the GaN epitaxial layer and PSS substrate and GaN surface and air [50, 51]. The reason why these oscillations are not seen in the estimated data is because the refractive index difference of the layers is not taken into account in the algorithm used.

Table 4 Model III train parameters

Hidden layer model	[5 10 20]
Train algorithm	Bayesian Neural Network
Momentum value	0.9
Train rate value	0.1
Train set temperature range (K)	[20 40 80 120 160 200 240 280]
Test set temperature range (K)	[60 100 140 180 220 260]
Data set wavelength range (nm)	[400 600]

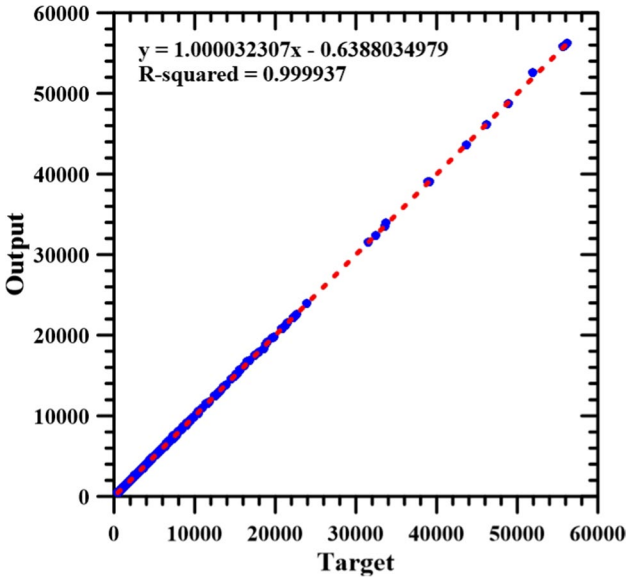

Fig. 8 Regression indicator for whole dataset in training of the model I

Establishment of artificial neural network model and training of the system

Two independent input variables and one dependent output variable given in Table 1 were obtained from experimental results.

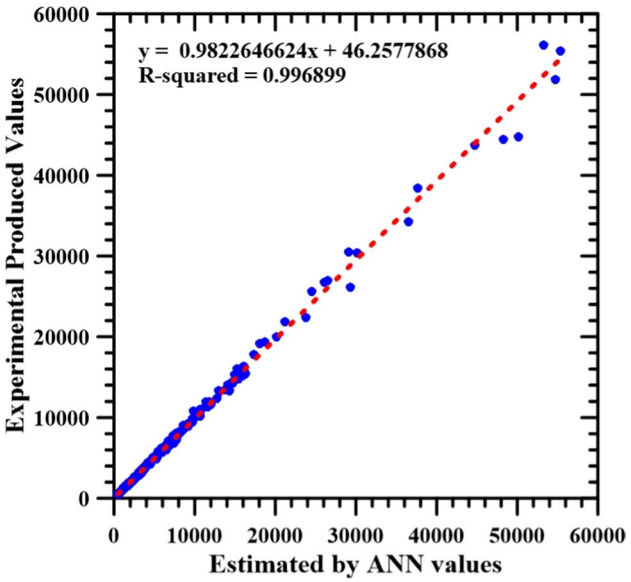

Fig. 9 Relationship between model I generated data and test dataset

Intensity values measured at different temperatures and different wavelengths with the established experimental setup were created for training the ANN model and designing the system, as shown in Fig. 6. These temperature values were measured at 14 different temperatures as (20, 40, 60, 80, 100, 120, 140, 160, 180, 200, 220, 240, 260, and 280 K), at minimum 330.06 and maximum 600 nm wavelengths.

When the graph of the data produced because of the experiments is examined, it is understood that the measurement results show different behavior in different intervals (Fig. 6). Modeling these effects not on the entire ANN system but at its own limits will increase the success of the system. For this reason, the system will be designed and trained as three different ANN models (named as model I, model II, and model III) that behave in different wavelength ranges (Fig. 7). Thus, the success of the system will support the experimental model at higher degrees. Model I is trained to generate intensity values produced at wavelengths between 340 and 370 nm. The values obtained in this range behave non-linearly. An ANN architecture is preferred to best model this behavior (Table 2). The model II is trained to generate intensity values produced at wavelengths between

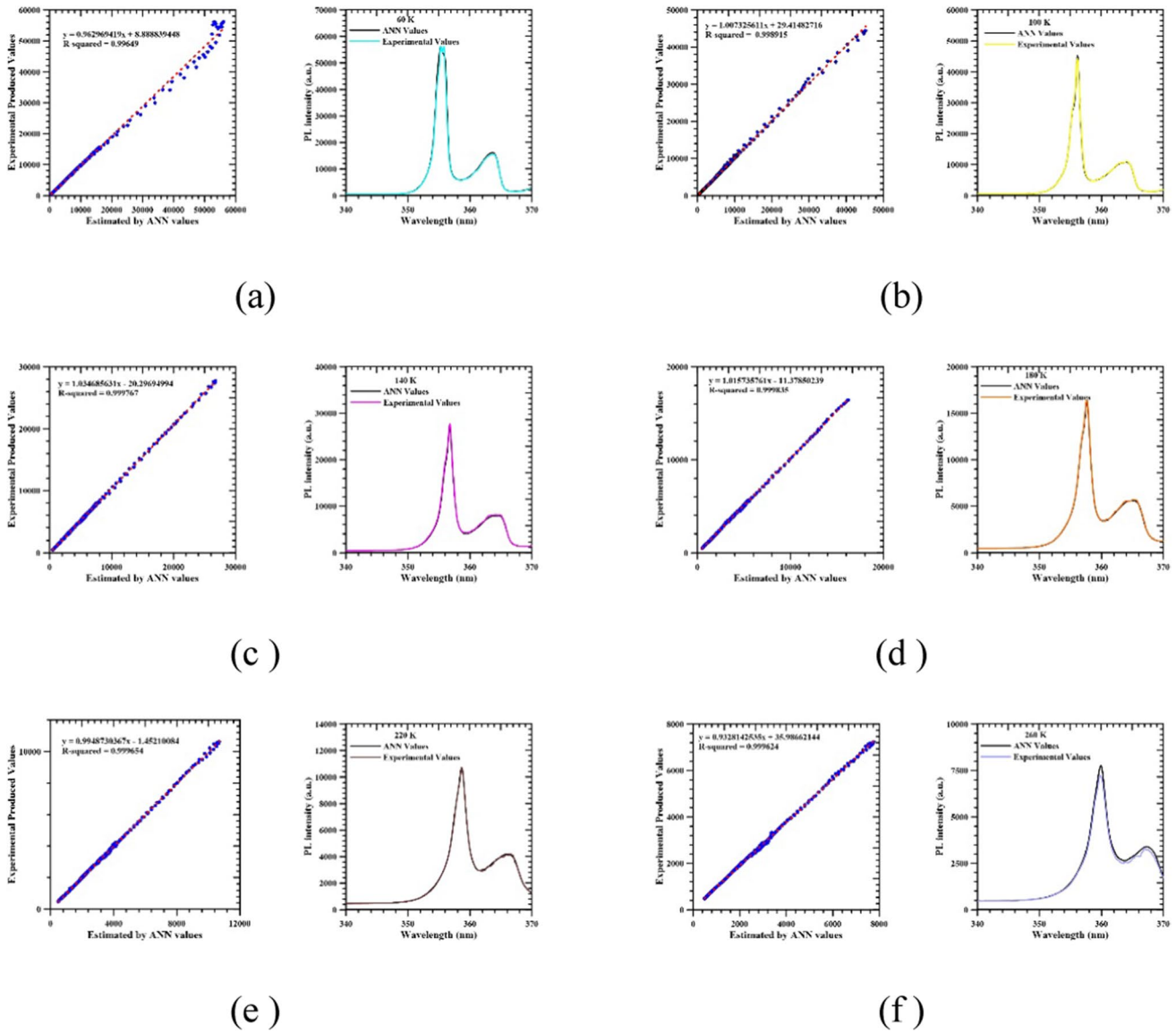

Fig. 10 (**a**) 60 K temperature results, (**b**) 100 K temperature results, (**c**) 140 K temperature results, (**d**) 180 K temperature results, (**e**) 220 K temperature results, and (**f**) 260 K temperature results

370 and 400 nm (Table 3) and the last, and model III is trained to generate intensity values produced at wavelengths between 400 and 600 nm (Table 4).

During the training of ANN models, the training dataset is divided into three parts to test the learning. ANN models, which offer good approximations, are directly related to the fact that the datasets used for their training represent the proposed problem. To protect the models developed within the framework of ANN from the disadvantages summarized in the previous sections, the training set should be fragmented and presented for training the model. If you want to construct a trustworthy ANN model, you need to separate your dataset into the training part, test part, and validation part sets. The training set is used to train and perform the model learn the hidden patterns in the dataset. The validation set is apart from the training set, and it is used to validate model performance during training phase. This validation operation serves information about that helps to tune the model's hyperparameters and configurations accordingly. The test set is used to test the model performance and truth after completing the training. The basic processing algorithms of the proposed model are carried out as summarized below.

1. All experimental data were recorded in the specified "Temperatures" and "Wavelengths" ranges
2. In this study, measurements were made for approximately fourteen temperature values
3. The created dataset is divided into three parts as datasets to be used in training the ANN model and testing the ANN model (temperature values are taken as the separation parameter)
4. The measurements of eight temperature values are reserved for the training of the models, and the measurements of six temperature values are reserved for the testing of the created models
5. Trainings were conducted using the training dataset created in step four on the determined ANN parameters.
6. The data values of the eight temperatures used during the trainings are specified in the model as 75% training, 15% validation, and 15% test during the training stages of the ANN
7. By updating the ANN parameters, the metrics were analyzed, and the most successful model was determined for the system to provide the optimum result
8. Model performance was verified over the values produced for the test data set determined in the 4th step by using various parameters over the trained ANN models

Training of the model in the 340–370-nm wavelength range (model I)

When the measurement data were examined, it was observed that the measurement results in this region are more variable.

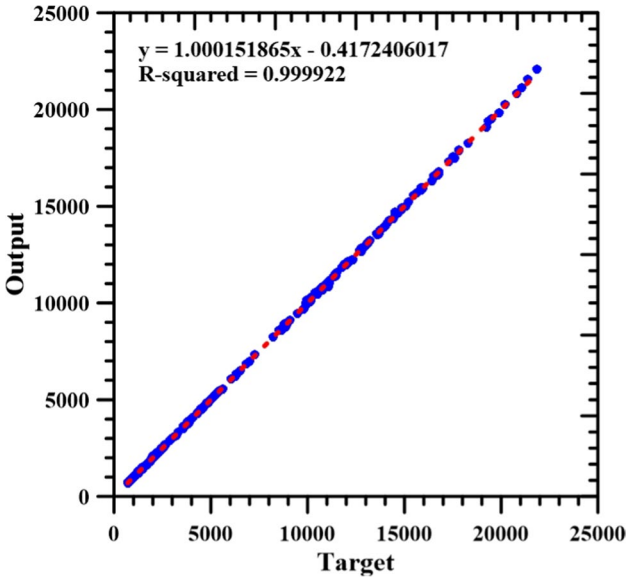

Fig. 11 Regression indicator for whole dataset in training of the model II

In the established ANN model, it is aimed to model these behaviors of the measurements in the best way. For this reason, the number of hidden layers in the artificial neural network model, which will affect the success of the system, and the number of neurons in the layers have been focused on.

The regression indicators of model 1 ($y - \hat{y}$) trained on the parameters shown in Table 2 were created with high performance as shown in Fig. 8. This model was obtained from the data presented to the system as a training set.

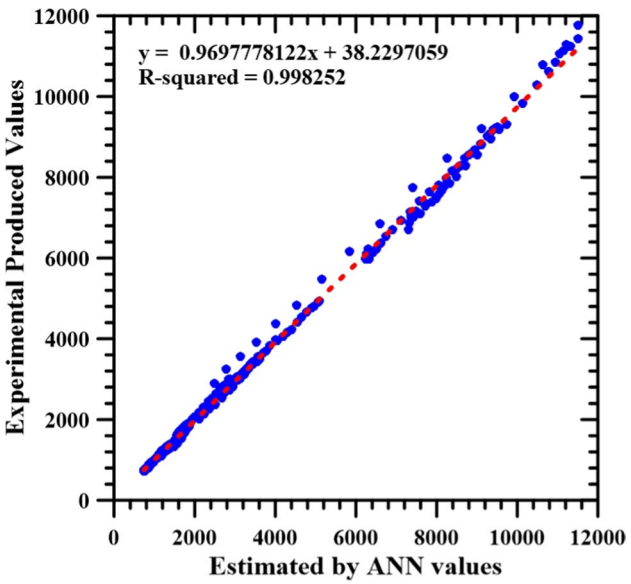

Fig. 12 Relationship between model II generated data and test dataset

The test data group, which was never presented in the training of the model, was presented to the developed ANN model to verify the performance of the model. When the outputs produced by the model were compared with the experimental outputs of the test data set, the success of the model was confirmed with the regression graph shown in Fig. 9. The most effective way to test system success is to examine the outputs generated by the model using data it has never seen. In other words, it is the similarity of the data measured in reality and the data produced by the ANN model.

As seen in Fig. 9 and understood from the *R* value, the trained ANN models the measurements in the study area at very high rates. In order to more clearly show the accuracy of the model, the outputs of the model and measured data for each temperature value in the test dataset are examined in the graphs in Fig. 10.

Training of the model in the 370–400-nm wavelength range (model II)

When the data in this range were trained together with those in the other ranges, significant deviations were observed, especially between the measured values and the predicted values. To protect the whole system from the effects of these deviations, the data was included in the system by training as model II in the range of 370–400.

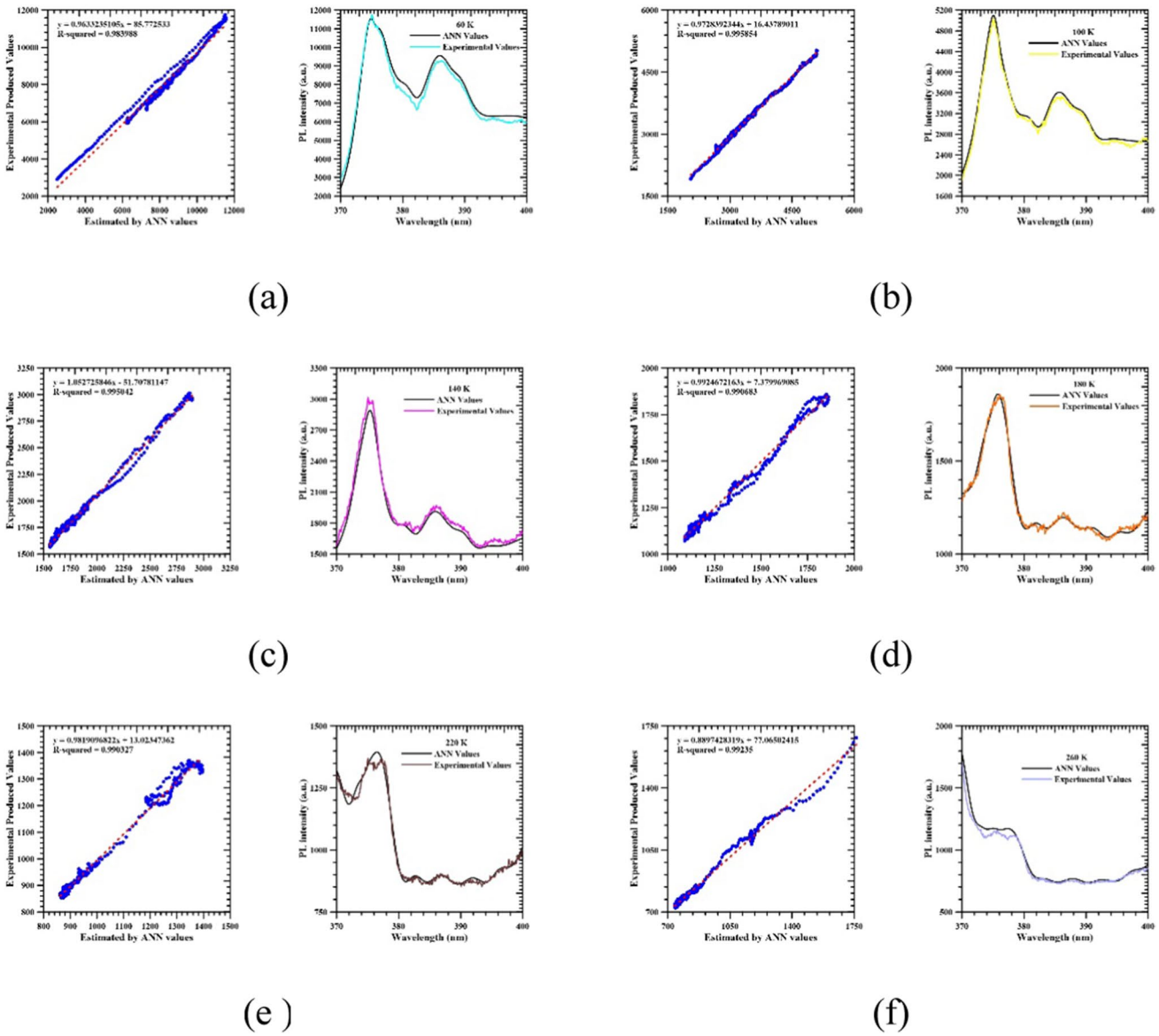

Fig. 13 (**a**) 60 K temperature results, (**b**) 100 K temperature results, (**c**) 140 K temperature results, (**d**) 180 K temperature results, (**e**) 220 K temperature results, and (**f**) 260 K temperature results

The representation rate of the results obtained was observed as more acceptable. The parameter values used for the training of model II are shown in Table 3. After the training is completed, the correlation graphs of the training data produced by model II are given in Fig. 11, and the correlation graphs of the test data are given in Fig. 12. Model and measured data for each temperature value in the test dataset are examined in the graphs in Fig. 13.

Training of the model in the 400–600-nm wavelength range (model III)

As can be seen from Fig. 6, experimental data in the 400–600 nm wavelength range show more linear behavior. For this reason, it is possible to train with a simpler ANN model. Such training will positively affect the calculation time and success of the system The regression indicators of model III ($y - \hat{y}$) trained on the parameters shown in Table 4 were created with high performance as shown in Fig. 14. This model was obtained from the data presented to the system as a training set.

When the outputs produced by the model were compared with the experimental outputs of the test data set, the success of the model was confirmed with the regression graph shown in Fig. 15.

The outputs of the model III and measured data for each temperature value in the test dataset are examined in the graphs in Fig. 16.

As it can be seen clearly from prepared three models, one of the key advantage of this study lies in the utilization of ANNs for the modeling of temperature-dependent PL of GaN epilayers. Unlike previous research which has explored various modeling techniques, including physical models and empirical fitting approaches, the application of ANNs specifically for this purpose is relatively unexplored. ANNs offer a data-driven approach that can capture complex non-linear relationships without the need for explicit physical models. By training on a large dataset comprising temperature and corresponding PL intensity values, the ANN model can learn the underlying patterns and make accurate predictions for unseen data points.

Conclusions

In the present study, first, PL measurements were carried out in different temperature ranges of the GaN layer grown by the MOCVD method. The data in the temperature values

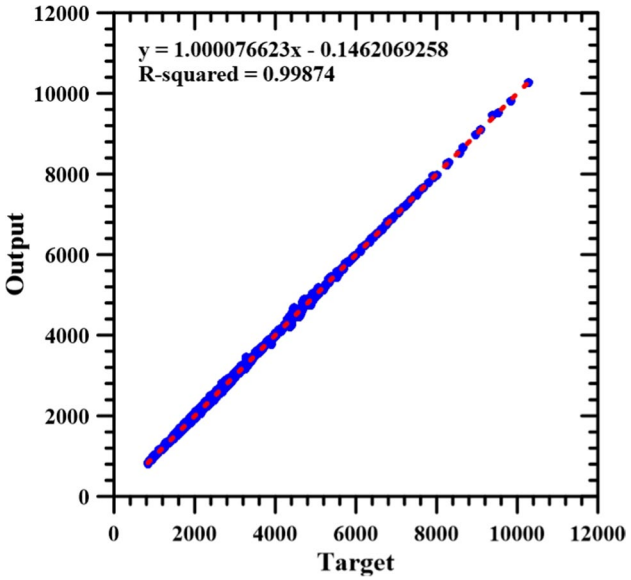

Fig. 14 Regression indicator for whole dataset in training of the model III

[20 40 80 120 160 200 240 280] were used for the training of three different models in the specified intervals, and the ANN model was created. To test the accuracy of the model, different temperature data, which were previously measured but never used in the training of the ANN, were used ([60 100 140 180 220 260]). 478 different measurement data in

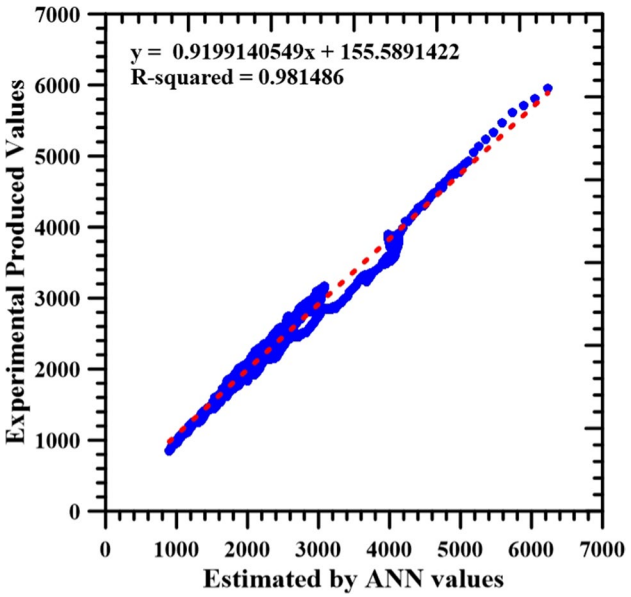

Fig. 15 Relationship between model III generated data and test dataset

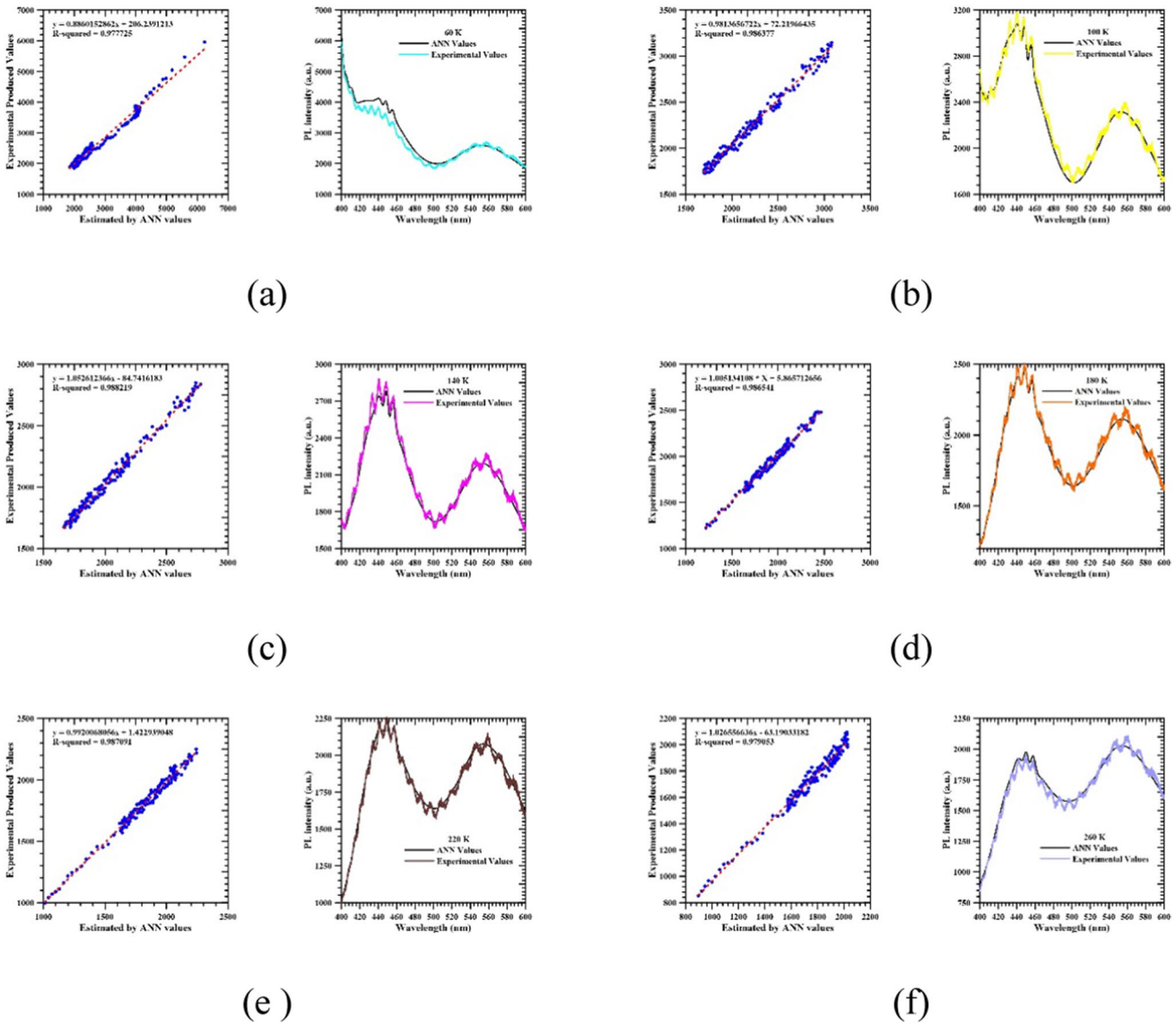

Fig. 16 (**a**) 60 K temperature results, (**b**) 100 K temperature results, (**c**) 140 K temperature results, (**d**) 180 K temperature results, (**e**) 220 K temperature results, and (**f**) 260 K temperature results

the 340–370-nm range, 478 different measurement data in the 370–400-nm range, and 3186 different measurement data in the 400–600-nm range are used.

One of the important optical characterizations is photoluminescence and its temperature dependent measurement. The temperature-dependent measurement of photoluminescence is disadvantageous in terms of both time and cost. Therefore, in this study, the ANN model has been studied to get rid of these disadvantages. Therefore, the PL behavior of the GaN layer has given us an important advantage in this sense. In other words, instead of making too many measurements experimentally, PL at the desired temperatures was estimated by applying the ANN model. As a result, it has been seen that accurate information about the optical behavior of GaN-based materials at different temperatures can be obtained. To prove it, the experimental data obtained and the ANN model were compared. While the ANN model was being developed, it was observed that the similarity rates of the outputs produced by the experimental and ANN models were high with the changes made on the system parameters of the ANN. The R^2 values of the test data produced convergent results very similar to the R^2 values of the training data.

For the first time in the literature, process models using ANN made it possible to predict results within unknown

(not experimentally obtained) temperature values by modeling intensity values at certain wavelengths for different temperature values made in this study. At the same time, it is possible to have information about the optical behavior of GaN-based materials at different temperatures by reducing the number of temperature-dependent PL measurements with the ANN model.

Acknowledgements This study is conducted in Sivas Cumhuriyet University R & D Center (CUTAM), Sivas Cumhuriyet University Nanophotonic Application and Research Center.

Author contribution Ebru Şenadım Tüzemen: supervision and review. Ahmet Gürkan Yüksek: conceptualization, investigation, and visualization. İlkay Demir: conceptualization, investigation, visualization, and writing— review and editing. Sabit Horoz: review and editing. İsmail Altuntaş: conceptualization, investigation, visualization, and writing— review and editing.

Data availability Not applicable.

Declarations

Consent to participate Not applicable.

Consent for publication Not applicable.

Competing interests The authors declare no competing interests.

References

1. Bryan, I., et al.: Doping and compensation in Al-rich AlGaN grown on single crystal AlN and sapphire by MOCVD. Appl. Phys. Lett. **112**(6), 062102 (2018)
2. Buzynin, Y.N., et al.: InN layers grown by MOCVD on a-plane Al2O3. Physica Status Solidi (a) **215**(11), 1700919 (2018)
3. Genç, M., et al.: Distributed contact flip chip InGaN/GaN blue LED; comparison with conventional LEDs. Superlattices Microstruct. **128**, 9–13 (2019)
4. O'leary, S.K., et al.: Steady-state and transient electron transport within the III–V nitride semiconductors, GaN, AlN, and InN: a review. J. Mater. Sci.: Mater. Electron. **17**(2), 87–126 (2006)
5. Garg, M., et al.: Giant UV photoresponse of GaN-based photodetectors by surface modification using phenol-functionalized porphyrin organic molecules. ACS Appl. Mater. Interfaces. **11**(12), 12017–12026 (2019)
6. Meneghini, M., et al.: A review on the reliability of GaN-based LEDs. IEEE Trans. Device Mater. Reliab. **8**(2), 323–331 (2008)
7. Tian, A., et al.: Design and growth of GaN-based blue and green laser diodes. Sci. China Mater. **63**(8), 1348–1363 (2020)
8. Robin, Y., et al.: High brightness ultraviolet light-emitting diodes grown on patterned silicon substrate. Mater. Sci. Semicond. Process. **90**, 87–91 (2019)
9. Zhang, B., et al.: Damage-free transfer of GaN-based light-emitting devices and reuse of sapphire substrate. ECS J. Solid State Sci. Technol. **9**(6), 065019 (2020)
10. Oh, J.-T., et al.: High efficiency ultraviolet GaN-based vertical light emitting diodes on 6-inch sapphire substrate using ex-situ sputtered AlN nucleation layer. Opt. Express **26**(5), 5111–5117 (2018)
11. Wang, T., et al.: Fabrication of high performance of AlGaN/GaN-based UV light-emitting diodes. J. Cryst. Growth **235**(1–4), 177–182 (2002)
12. Akasaki, I., et al.: Growth of GaN and AlGaN for UV/blue pn junction diodes. J. Cryst. Growth **128**(1–4), 379–383 (1993)
13. Shan, W., et al.: Temperature dependence of interband transitions in GaN grown by metalorganic chemical vapor deposition. Appl. Phys. Lett. **66**(8), 985–987 (1995)
14. Strite, S., et al.: An investigation of the properties of cubic GaN grown on GaAs by plasma-assisted molecular-beam epitaxy. J. Vac. Sci. Technol. B: Microelectron. Nanometer Struct Process. Meas. Phenom. **9**(4), 1924–1929 (1991)
15. Wolff, N., et al.: Advanced hybrid GaN/ZnO nanoarchitectured microtubes for fluorescent micromotors driven by UV light. Small **16**(2), 1905141 (2020)
16. Zhao, Y., et al.: Optical properties evolution of GaN film grown via lateral epitaxial overgrowth. Appl. Surf. Sci. **513**, 145816 (2020)
17. Rouet-Leduc, B., et al.: Optimisation of GaN LEDs and the reduction of efficiency droop using active machine learning. Sci. Rep. **6**(1), 1–6 (2016)
18. Shtepliuk, I., et al.: Excitonic emission in heavily Ga-doped zinc oxide films grown on GaN. J. Lumin. **223**, 117265 (2020)
19. Almeida, G.F.B.D., et al.: Incubation effect during laser micromachining of GaN films with femtosecond pulses. J. Mater. Sci.: Mater. Electron. **30**(18), 16821–16826 (2019)
20. Altuntas, İ: XRD and photoluminescence measurements of GaN grown on dome shaped patterned sapphire with different NH3 flow rates. Cumhuriyet Sci. J. **42**(1), 184–190 (2021)
21. Song, S., et al.: Improvement of quality and strain relaxation of GaN epilayer grown on SiC substrate by in situ SiNx interlayer. J. Mater. Sci.: Mater. Electron. **24**(8), 2923–2927 (2013)
22. Uma, M., et al.: Effect of rare-earth Pr6O11 insulating layer on the electrical properties of Au/n-GaN Schottky electrode and its chemical and structural characterization. J. Mater. Sci.: Mater. Electron. **30**(20), 18710–18719 (2019)
23. Maskar, E., et al.: A DFT study of electronic, magnetic, optical and transport properties of rare earth element (Gd, Sm)-doped GaN material. Mater. Sci. Semicond. Process. **139**, 106326 (2022)
24. Bilgili, A.K., et al.: A detailed study on optical properties of InGaN/GaN/Al2O3 multi quantum wells. J. Mater. Sci.: Mater. Electron. **30**(11), 10391–10398 (2019)
25. Johar, M.A., et al.: Universal and scalable route to fabricate GaN nanowire-based LED on amorphous substrate by MOCVD. Appl. Mater. Today **19**, 100541 (2020)
26. Zhou, S., et al.: The effect of nanometre-scale V-pits on electronic and optical properties and efficiency droop of GaN-based green light-emitting diodes. Sci. Rep. **8**(1), 1–12 (2018)
27. Torun, Y., et al.: Modeling of Schottky diode characteristic by machine learning techniques based on experimental data with wide temperature range. Superlattices Microstruct. **160**, 107062 (2021)
28. Wang, Z., et al.: A machine learning-assisted model for GaN ohmic contacts regarding the fabrication processes. IEEE Trans. Electron Devices **68**(5), 2212–2219 (2021)
29. Arteev, D.S., et al.: Implementation of an artificial neural network to predict properties of MOVPE-grown AlGaN layers. IOP Conf. Ser.: J. Phys. Conf Ser. **1199**, 012007 (2019)
30. Soltani, S., et al.: Luminescence dynamics in AlGaN with AlN content of 20%. Phys. Status Solidi A **214**(4), 1600481 (2017)
31. Chowdhury, A.M., et al.: Temperature dependent "S-shaped" photoluminescence behavior of InGaN nanolayers: optoelectronic implications in harsh environment. ACS Appl. Nano Mater. **3**(8), 8453–8460 (2020)

32. Yüksek, A.G., et al.: Modeling of reflectance properties of ZnO film using artificial neural networks. J. Optoelectron. Adv. Mater. **17**(11–12), 1615–1628 (2015)
33. Altuntas, I., et al.: The effects of two-stage HT-GaN growth with different V/III ratios during 3D–2D transition. J. Phys. D Appl. Phys. **51**(3), 035105 (2017)
34. Demir, I., et al.: Microstructural evolution of MOVPE grown GaN by the carrier gas. Semiconductors **52**(16), 2030–2038 (2018)
35. Mollalo, A., et al.: Artificial neural network modeling of novel coronavirus (COVID-19) incidence rates across the continental United States. Int. J. Environ. Res. Public Health **17**(12), 4204 (2020)
36. Yüksek, A. G., et al.: Comparison of the effects dimensionalty methods in the training of neuro-fuzzy (ANFIS) classifications. In: 2017 International Artificial Intelligence and Data Processing Symposium (IDAP). IEEE, p. 1–9 (2017)
37. Serin, G., et al.: Review of tool condition monitoring in machining and opportunities for deep learning. Int. J. Adv. Manuf. Technol. **109**(3), 953–974 (2020)
38. Ahmad, F., et al.: Machine learning-integrated omics for the risk and safety assessment of nanomaterials. Biomater. Sci. **9**(5), 1598–1608 (2021)
39. Qiu, Y., et al.: An artificial neural network model to predict mini/micro-channels saturated flow boiling heat transfer coefficient based on universal consolidated data. Int. J. Heat Mass Transf. **149**, 119211 (2020)
40. RAUT, Rakesh D., et al.: Linking big data analytics and operational sustainability practices for sustainable business management. J. Clean. Prod. **224**, 10–24 (2019)
41. Ma, X., et al.: Structural damage identification based on unsupervised feature-extraction via variational auto-encoder. Measurement **160**, 107811 (2020)
42. Ferentinos, K.: Deep learning models for plant disease detection and diagnosis. Comput. Electron. Agric. **145**, 311–318 (2018)
43. Zuo, C., et al.: Deep learning in optical metrology: a review. Light: Sci. Appl. **11**(1), 1–54 (2022)
44. Aghbashlo, M., et al.: Machine learning technology in biodiesel research: a review. Prog. Energy Combust. Sci. **85**, 100904 (2021)
45. Kayri, M.: Predictive abilities of Bayesian regularization and Levenberg–Marquardt algorithms in artificial neural networks: a comparative empirical study on social data. Math. Comput Appl **21**(2), 20 (2016)
46. Theocharides, S., et al.: Day-ahead photovoltaic power production forecasting methodology based on machine learning and statistical post-processing. Appl. Energy **268**, 115023 (2020)
47. Ghadai, M., et al.: Artificial neural network and weighted arithmetic indexing approach for surface water quality assessment of the Brahmani river. Glob. Nest J. **24**(4), 562–568 (2022)
48. Hu, X.: DB-HReduction: a data preprocessing algorithm for data mining applications. Appl. Math. Lett. **16**, 889–895 (2003)
49. Reshchikov, M.A., et al.: Two yellow luminescence bands in undoped GaN. Sci. Rep. **8**(1), 1–11 (2018)
50. Lee, T.G., et al.: Fabry-Perot interference characteristics of the photoluminescence in nanoclustered SiNx: H thick films. J. Korean Phys. Soc. **50**(3), 581–585 (2007)
51. Hums, C., et al.: Fabry-Perot effects in InGaN/GaN heterostructures on Si-substrate. J. Appl. Phys. **101**(3), 033113 (2007)